

# Meson-exchange currents and quasielastic predictions for neutrino-nucleus scattering

**Maria Barbaro**

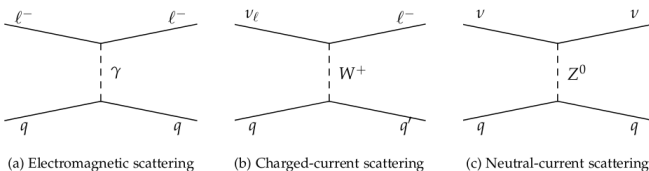
Dipartimento di Fisica and INFN, Torino, Italy

**NUFACT2017**

September 25-30, 2017, Uppsala

# Outline

- 1 Connection between  $\nu$ -A and e-A scattering: SuperScaling
- 2 Meson-exchange currents: the 2p2h response
- 3 Results
- 4 Conclusions



- Neutrino- and electron-nucleus scattering are obviously connected to each other and a reliable model must be able to describe both processes.  
However:

- Neutrinos can probe both the **vector** and **axial** nuclear responses, unlike (unpolarized) electrons, which are sensitive only to the vector response
- The experimental conditions are different:
  - **$(e, e')$** : the electron energy is well determined and different mechanisms can be clearly identified by knowing the energy and momentum transfer
  - **$CC(\nu_\ell, l)$** :  $E_\nu$  is broadly distributed in the neutrino beam and different mechanisms can contribute to the same kinematics of the outgoing lepton

→ Although not sufficient to fully constrain neutrino cross sections, electron scattering is a **necessary test for nuclear models**.

# The SuperScaling approach

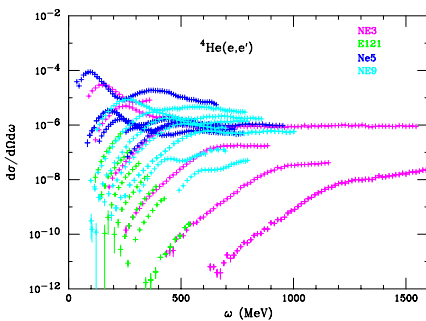
- Many high quality  $e - A$  data exist, which must be used to **test** models, and can also be used as an **input** for predicting  $\nu$ -A observables.
- The SuperScaling approach exploits **universal features** of lepton-nucleus scattering to connect the two processes.
- Scaling occurs when a function of 2 variables becomes a function of only 1 variable, called scaling variable (ex: Bjorken scaling).
- In lepton-nucleus scattering two kinds of scaling can be defined [Day *et al.*, ARNPS (1990), Donnelly and Sick, PRL82 & PRC60 (1999)]:  
“**Superscaling**” is the simultaneous occurrence of scaling of first and second kinds

- **Scaling of first kind:** the reduced cross section

$$F(q, \omega) \equiv \frac{d^2\sigma/d\omega d\Omega}{\sigma_{Mott} (v_L G_L + v_T G_T)} \longrightarrow F(y)$$

i.e. the ddcs divided by an appropriate single-nucleon function, is independent of  $q$  if plotted versus the scaling variable

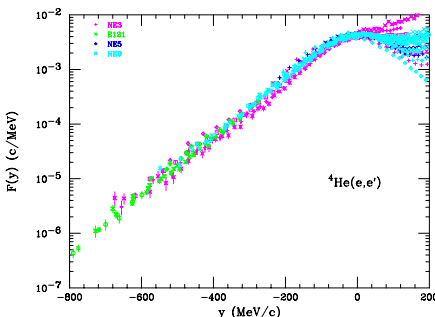
$$y(q, \omega) = -p_{min}$$



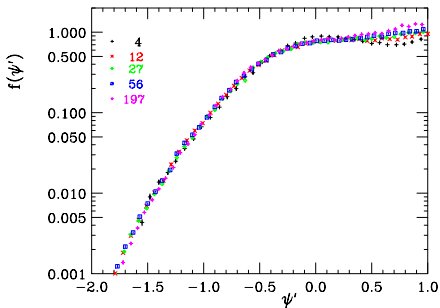
- Scaling occurs when a function of 2 variables becomes a function of only 1 variable, called scaling variable (ex: Bjorken scaling). In lepton-nucleus scattering two kinds of scaling can be defined:
- Scaling of first kind:** the reduced cross section

$$F(q, \omega) \equiv \frac{d^2\sigma/d\omega d\Omega}{\sigma_{Mott}(\nu_L G_L + \nu_T G_T)} \longrightarrow F(y)$$

i.e. the ddcs divided by an appropriate single-nucleon function, is independent of  $q$  if plotted versus the scaling variable  $y(q, \omega) = -p_{min}$



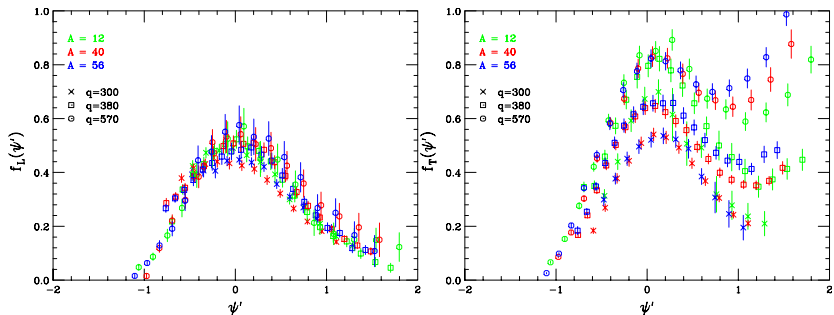
- **Scaling of second kind:** the reduced cross section multiplied by  $k_F$  is independent of the specific nucleus:  $f(y) = k_F \times F(y)$



- The **scaling variable  $\psi$**  is the relativistic version of  $y$  and  $\psi \simeq -y/k_F$
- **Superscaling** is the simultaneous occurrence of both kinds of scaling.
- Superscaling is fulfilled at energy loss below the QEP ( $\psi < 0$ ) and broken at  $\psi > 0$

## Superscaling in the Longitudinal and Transverse channels

- Define  $f_L = k_F R_L / G_L$  and  $f_T = k_F R_T / G_T$  and look at separated L/T data



- $f_T > f_L$
- Violations reside mainly in the transverse channel (2p2h MEC,  $\Delta$  resonance excitation, DIS, ...)
- The **RFG model** predicts  $f_L(\psi) = f_T(\psi) = \frac{3}{4}(1 - \psi^2)\theta(1 - \psi^2)$ , in **disagreement with the experimental data**

## Neutrino-nucleus scattering: response functions

- Double differential CC  $\nu$  (+) and  $\bar{\nu}$  (-) **inclusive** cross section ( $\nu_I, l'$ )

$$\left[ \frac{d\sigma}{dk_\mu d\Omega} \right]_{\pm} = \sigma_0 \mathcal{F}_{\pm}^2 \quad ; \quad \sigma_0 = \frac{(G_F^2 \cos \theta_c)^2}{2\pi^2} \left( k_\mu \cos \frac{\theta}{2} \right)^2$$

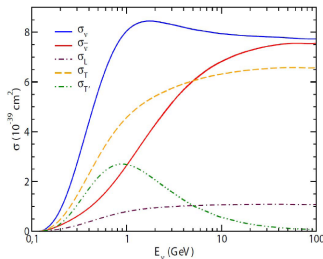
- Rosenbluth-like decomposition: 5 responses (components of the nuclear tensors)

$$\begin{aligned} \mathcal{F}_{\pm}^2 &= \hat{V}_L R_L + \hat{V}_T R_T \pm [2 \hat{V}_{T'} R_{T'}] \\ \hat{V}_L R_L &= V_{CC} R_{CC} + V_{CL} R_{CL} + V_{LL} R_{LL} \end{aligned}$$

with

$$\begin{aligned} R_L &= R_L^{VV} + R_L^{AA} && \text{VV (vector-vector)} \\ R_T &= R_T^{VV} + R_T^{AA} && \text{AA (axial-axial)} \\ R_{T'} &= R_{T'}^{VA} && \text{VA (vector-axial)} \end{aligned}$$

from the V and A weak leptonic and hadronic currents  $j^\mu = j_V^\mu + j_A^\mu$  ;  $J^\mu = J_V^\mu + J_A^\mu$

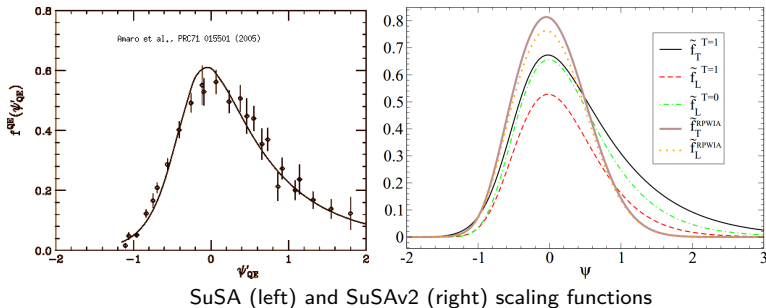


- Each response can be calculated as  $R^K = \frac{1}{k_F} G^K \times f^K$

- Note that for semi-inclusive reactions ( $\nu_I, l/N$ ) the responses are 10

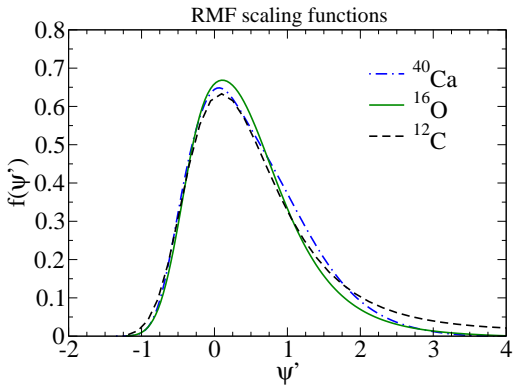
# The SuSAv2 model

- The **SuSA** model is based on the quasielastic longitudinal superscaling function extracted from averaged separated (e,e') world data on  $^{12}\text{C}$ ,  $^{40}\text{Ca}$ ,  $^{56}\text{Fe}$  and assumes  $f_L = f_T$  [Amaro et al., PRC71 (2005)]
- In the **SuSAv2** the scaling functions are calculated within the **Relativistic Mean Field** model, which predicts, for instance, different scaling functions in the L and T channels and in different isospin channels [Gonzalez et al., PRC90 (2014); Megias et al., PRD94 (2016)]
- The well-known shortcoming of RMF of being too strong at high energies is corrected for by introducing a q-dependent blending function which mixes RMF and RPWIA (two parameters)



# The SuSAv2 model for different nuclei

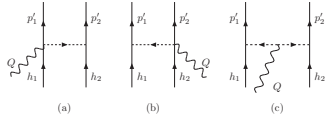
- 2-nd kind scaling within the RMF and RPWIA models
- $k_F$  and  $E_{shift}$  are the only different parameters



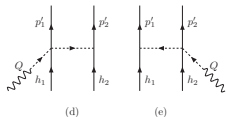
# Meson-exchange currents: the 2p2h response

- In our model the MEC are carried by the pion and  $\Delta$  degrees of freedom:

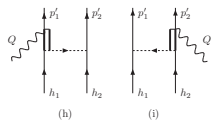
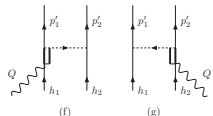
“Seagull” and  
“Pion-in-flight”



“Pion-pole”



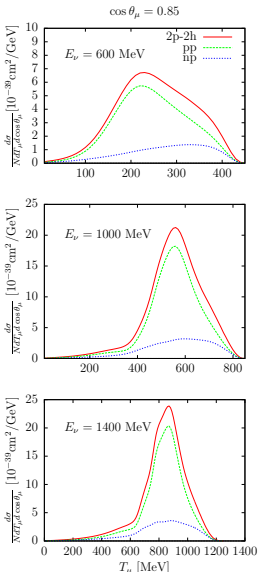
“ $\Delta$ -MEC”



# Meson-exchange currents: the 2p2h response

- The 2p2h model is based on the calculation performed by A. De Pace et al., (2003) for electron scattering, recently extended to the weak sector [I. Ruiz Simo et al., (2016)]
- All 2p-2h many-body diagrams containing two pionic lines are included (thousands of terms).
- The calculation is performed in the Relativistic Fermi Gas basis in which Lorentz covariance can be maintained.
- Although based on the simple RFG, it is computationally non-trivial and involves 7D integrals of many terms. Comparison with neutrino scattering data implies one additional integral over the neutrino flux.
- Two different techniques were used:
  - De Pace et al.: polarization propagator, many-body Goldstone diagrams, analytic manipulation of isospin traces and Dirac matrices spin traces using FORM, Monte Carlo integration.
  - Amaro et al.: numerical evaluation of the hadronic tensor  $W_{2p2h}^{\mu\nu}$ , including the spin traces.
  - Although the two methods are completely equivalent, the second has some practical advantages, like the possibility of separating the pp, nn, pn channels.

# Separated charge channels in the 2p2h response



- pp final state largely dominate over np
- The ratio depends upon the kinematics
- The np cross section is shifted towards higher values of  $T_\mu$
- First step towards the treatment of  $Z \neq N$  nuclei

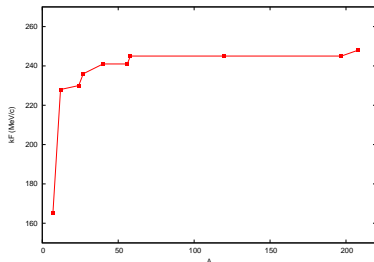
[Ruiz Simo et al., PLB762 (2016)]

## Density dependence of 2p2h meson-exchange currents

- Most existing calculations of 2p2h MEC refer to  $^{12}\text{C}$ .
- Other nuclei are interesting for oscillation experiments (mainly  $^{16}\text{O}$ ,  $^{40}\text{Ar}$ ).
- In the SuSA model each nucleus is characterized by two parameters:  $k_F$  and  $E_{shift}$ , fitted to reproduce the width and position of the QEP in inclusive electron scattering

TABLE I. Adjusted parameters.

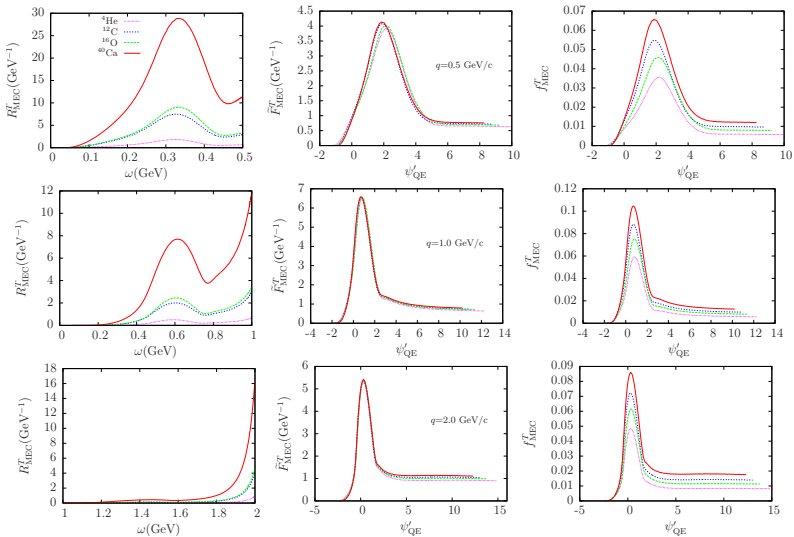
Nucleus	$k_F$ (MeV/c)	$E_{shift}$ (MeV)
Lithium	165	15
Carbon	228	20
Magnesium	230	25
Aluminum	236	18
Calcium	241	28
Iron	241	23
Nickel	245	30
Tin	245	28
Gold	245	25
Lead	248	31



Maierov, Donnelly, Sick, PRC65 (2002)

 $k_F(A)$

## Density dependence of 2p2h meson-exchange currents, Amaro et al., PRC95 (2017), 065502

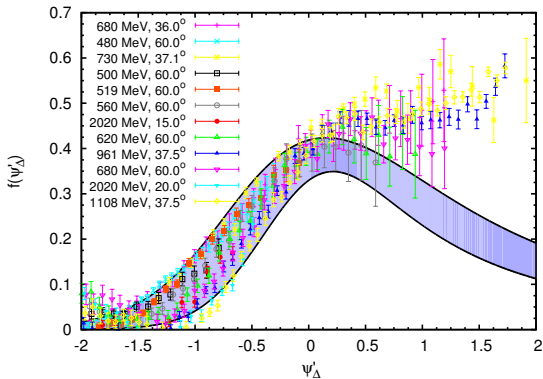


$$\tilde{F}_{\text{MEC}}^T \equiv \frac{R_{\text{MEC}}^T}{\frac{G_M^2(\tau)}{G_M^2(\tau)} \frac{m_N^2}{k_F^2}}; \quad f_{\text{MEC}}^T \equiv \frac{R_{\text{MEC}}^T}{\frac{G_M^2(\tau)}{G_M^2(\tau)} \frac{k_F}{m_N}} \implies \text{the 2p2h response scales as } k_F^2, \text{ while the QE response scales as } 1/k_F$$

## The inelastic region

The Superscaling approach can be extended to the inelastic spectrum in two ways:

- employing phenomenological fits of the single-nucleon inelastic structure functions and assuming that the scaling function is the same in all energy regions → full spectrum (from the  $\Delta$  resonance to DIS) [MBB et al., PRC69 (2004); Megias et al., PRD94 (2016)]
- constructing a phenomenological scaling function to be used in the  $\Delta$ -resonance region by subtracting from the inclusive ( $e, e'$ ) data the QE contribution and dividing the results by the appropriate  $N \rightarrow \Delta$  elementary function [Ivanov et al., PLB711 (2012)]



## Results

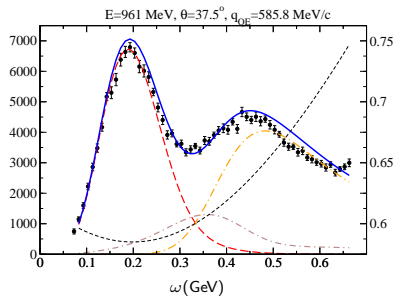
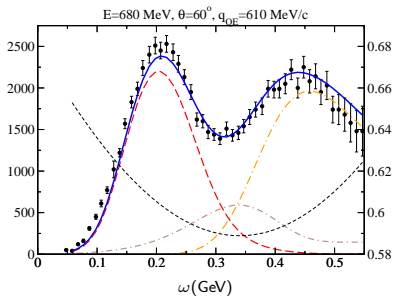
- Inclusive electron scattering on Carbon and Oxygen
- T2K CCQE-like  $\nu_\mu$  and  $\bar{\nu}_\mu$  on Carbon and Oxygen
- T2K CC inclusive  $\nu_\mu$  and  $\nu_e$  on Carbon
- MINER $\nu$ A CCQE-like  $\nu_\mu$ ,  $\bar{\nu}_\mu$ ,  $\nu_e$  and  $\bar{\nu}_e$  on Carbon
- MiniBooNE CCQE-like  $\nu_\mu$  and  $\bar{\nu}_\mu$  on Carbon

## **Inclusive electron scattering on Carbon and Oxygen**

# e-Carbon

## Validation: electron scattering data on Carbon

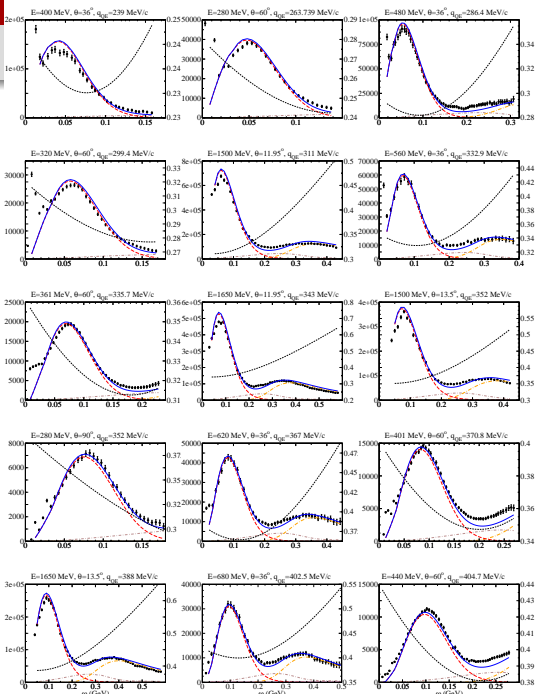
Megias *et al.*, PRD 94, 013012 (2016)



e-C data from Day *et al.*, <http://faculty.virginia.edu/qes-archive/>

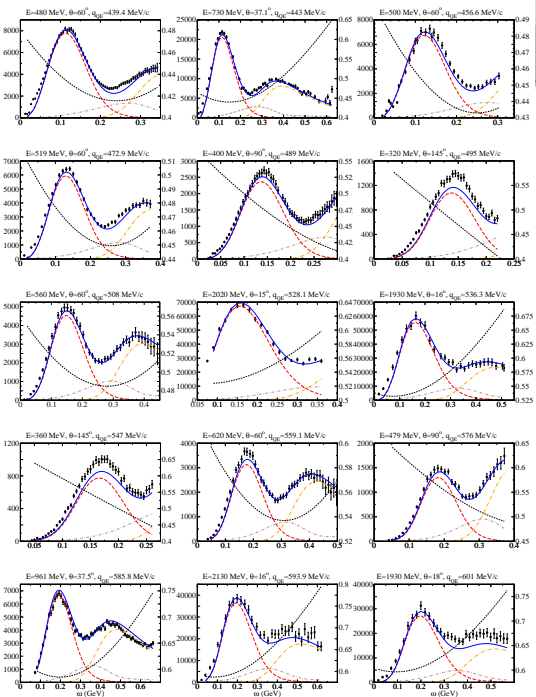
# e-Carbon

$q \sim 0.2\text{--}0.4 \text{ GeV}/c$



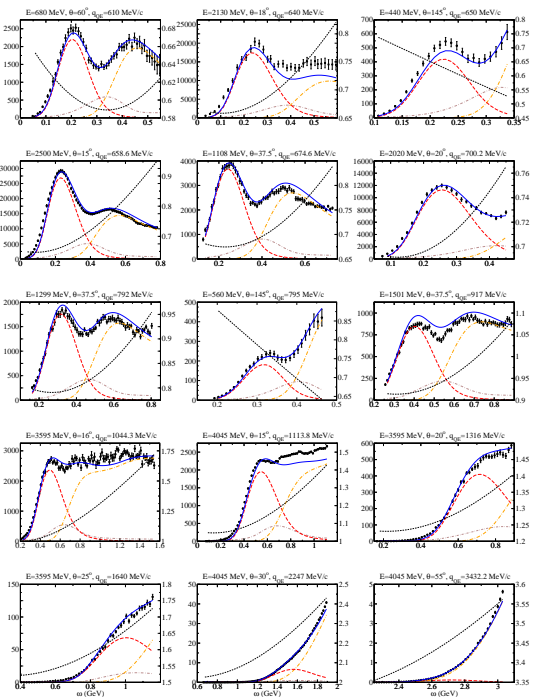
# e-Carbon

$q \sim 0.4\text{--}0.6 \text{ GeV}/c$



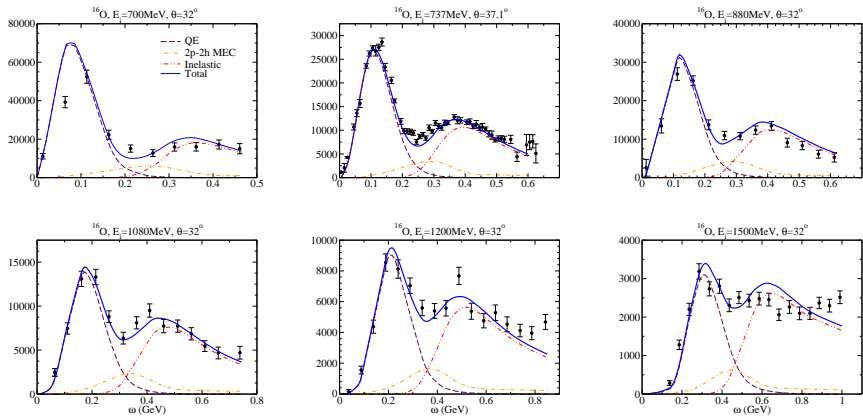
# e-Carbon

$q \sim 0.6\text{--}3.5 \text{ GeV}/c$



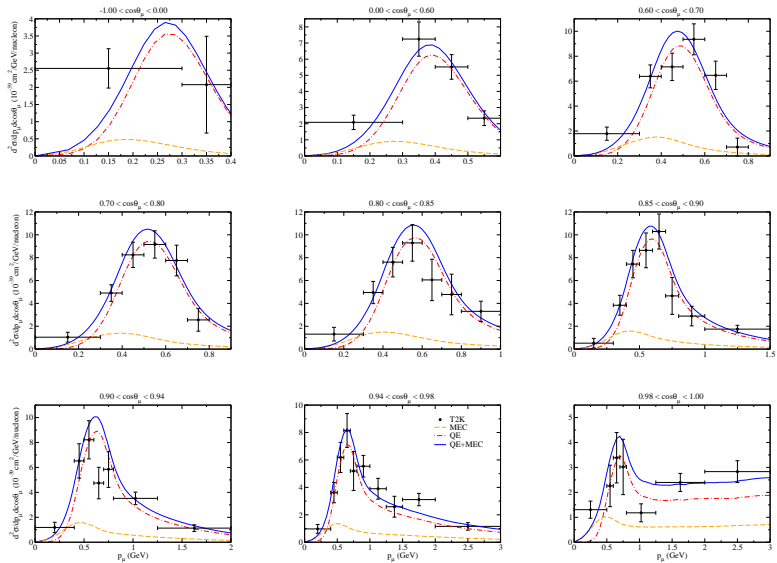
# e-Oxygen

Validation: electron scattering data on Oxygen (few data)

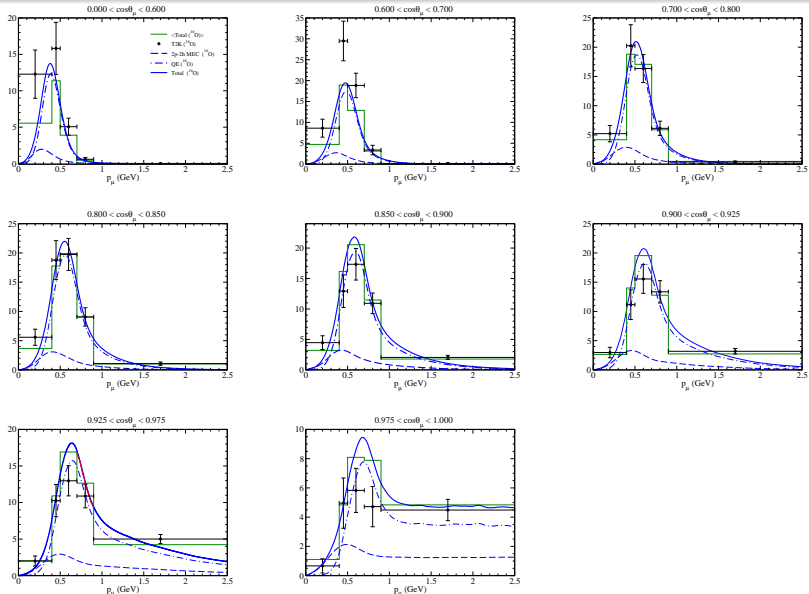


T2K

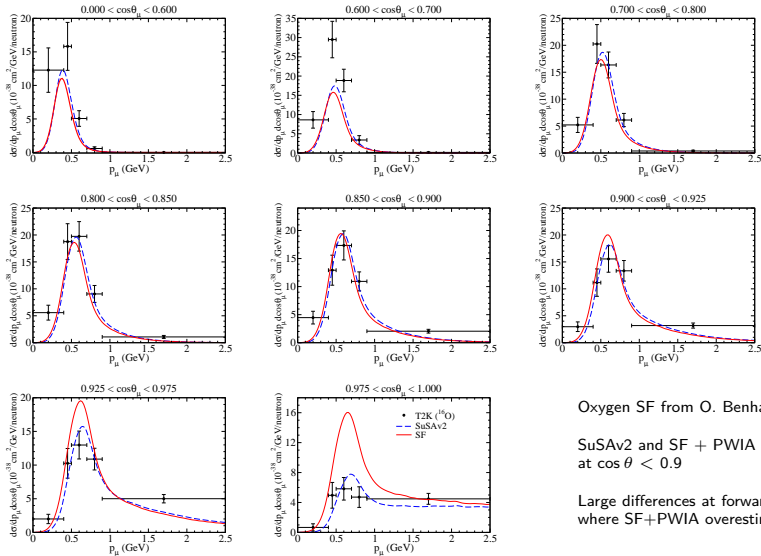
# T2K CC0 $\pi$ $\nu_\mu$ -C in the SuSAv2-MEC model



# T2K CC $\bar{\nu}_\mu$ -O in the SuSAv2-MEC model



# T2K CCQE $\nu_\mu$ -O in the Spectral Function PWIA approximation

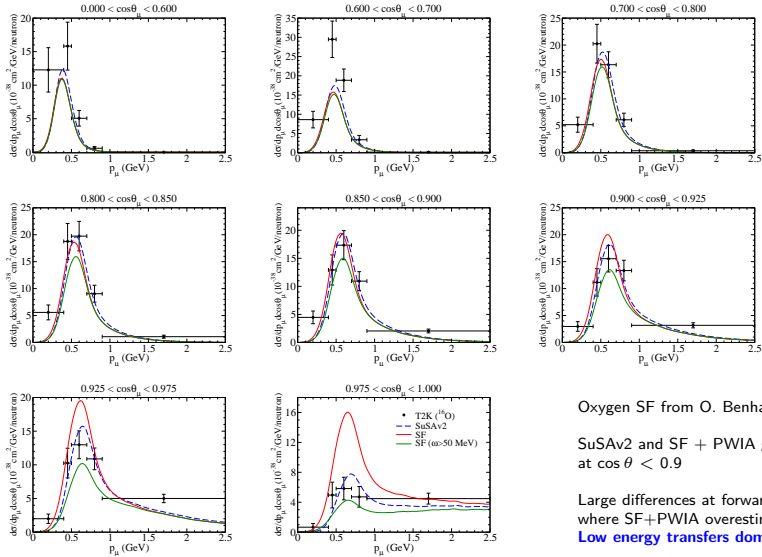


Oxygen SF from O. Benhar

SuSAv2 and SF + PWIA give similar results at  $\cos\theta < 0.9$

Large differences at forward angles, where SF+PWIA overestimates the data

# T2K CCQE $\nu_\mu$ -O in the Spectral Function PWIA approximation

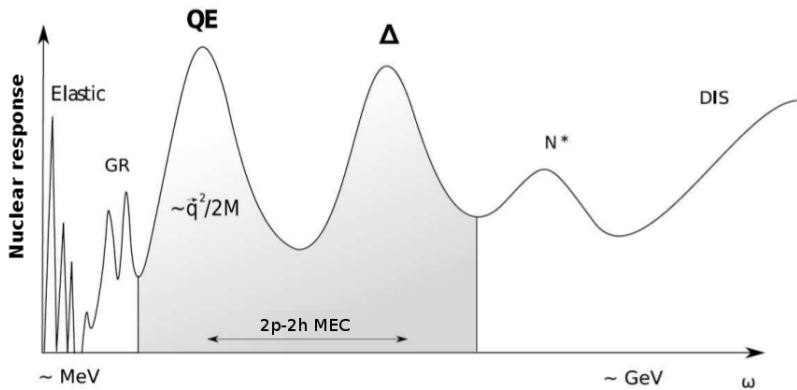


Oxygen SF from O. Benhar

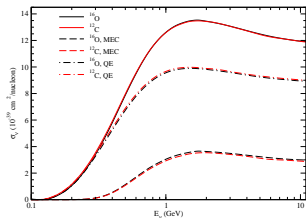
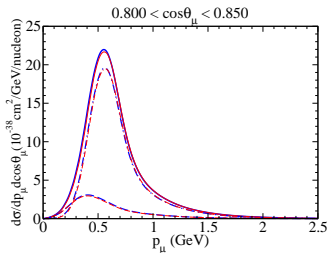
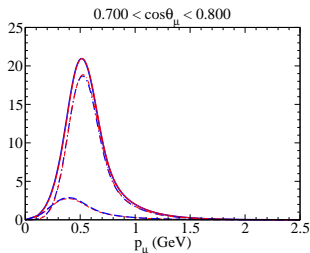
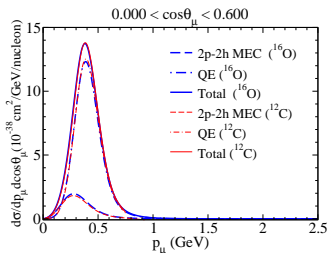
SuSAv2 and SF + PWIA give similar results at  $\cos\theta < 0.9$

Large differences at forward angles,  
where SF+PWIA overestimates the data  
**Low energy transfers dominate at small angles**

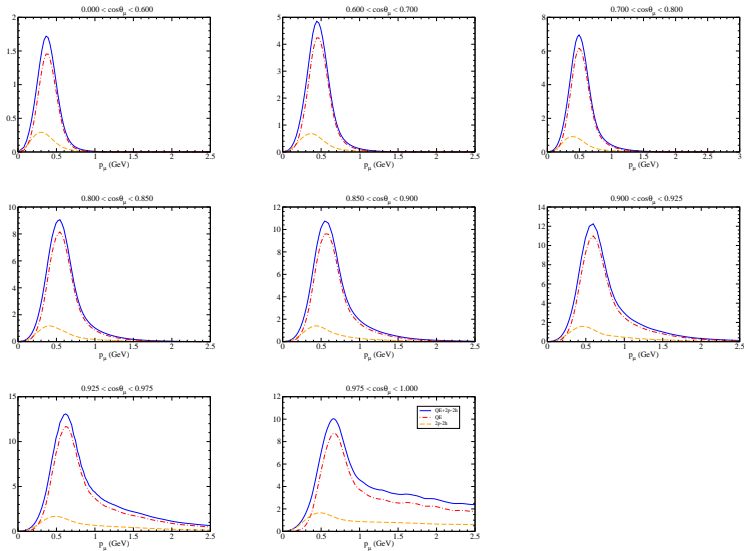
# Energy regimes of the nuclear response



# Carbon vs Oxygen

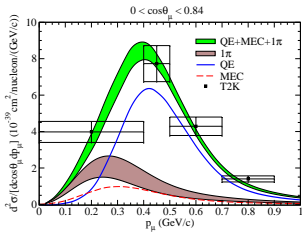
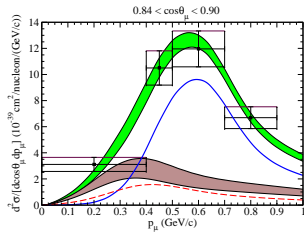
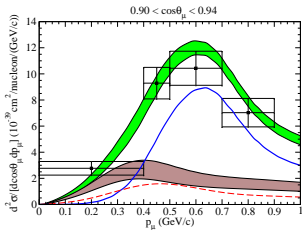
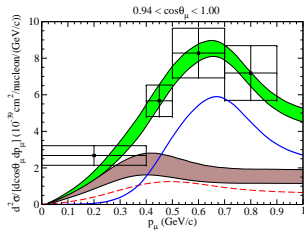


# T2K CC0 $\pi$ $\bar{\nu}_\mu$ -O predictions in the SuSAv2-MEC model



T2K inclusive  $\nu_\mu$ -C $\langle E_{\nu_\mu} \rangle \sim 0.8 \text{ GeV}$ 

Megias et al., PRD 94, 093004 (2016)

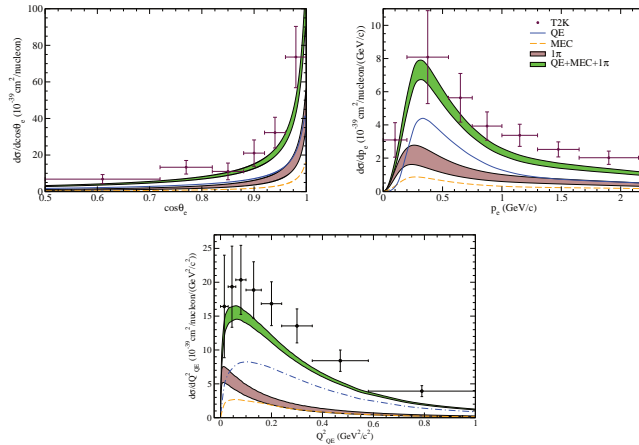


QE+MEC+1π model compatible with data

T2K inclusive  $\nu_e$ -C

$$\langle E_{\nu_e} \rangle \sim 1.3 \text{ GeV}$$

Megias et al., PRD 94, 093004 (2016)

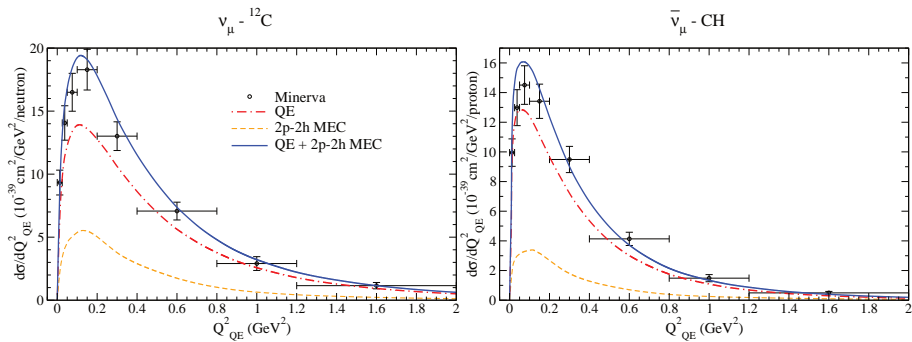


QE+MEC+ $1\pi$  model-data agreement is slightly worse, DIS starts being relevant

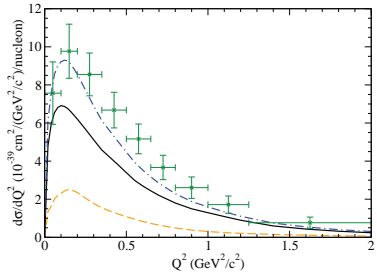
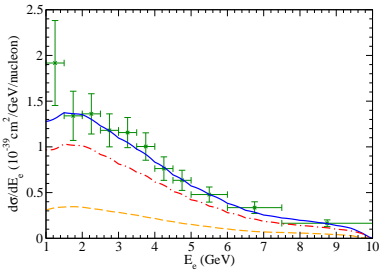
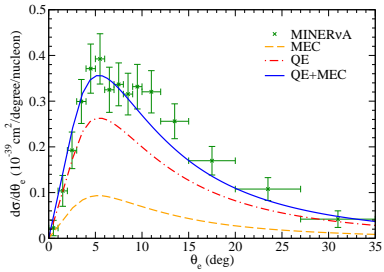
**MINER $\nu$ A**

# MINER $\nu$ A CCQE-like $\nu_\mu$ -C and $\bar{\nu}_\mu$ -C

Megias *et al.*, PRD 94, 093004 (2016)



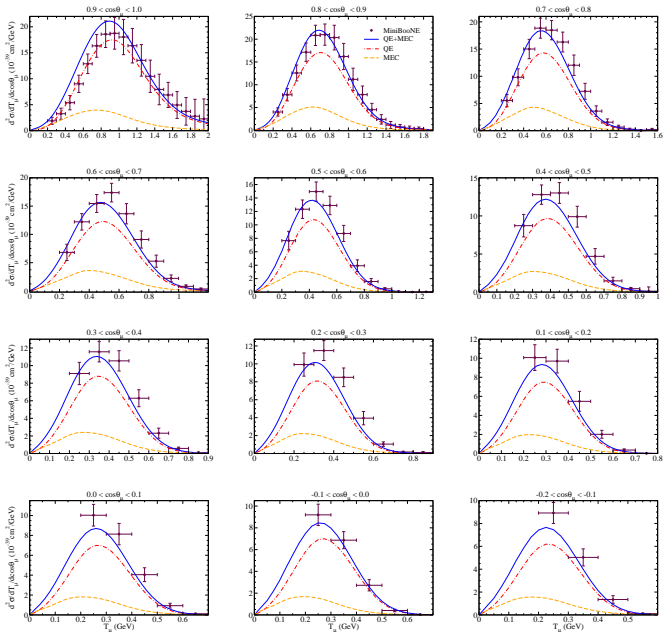
# Miner $\nu$ A CCQE-like $\nu_e$ -C



**MiniBooNE**

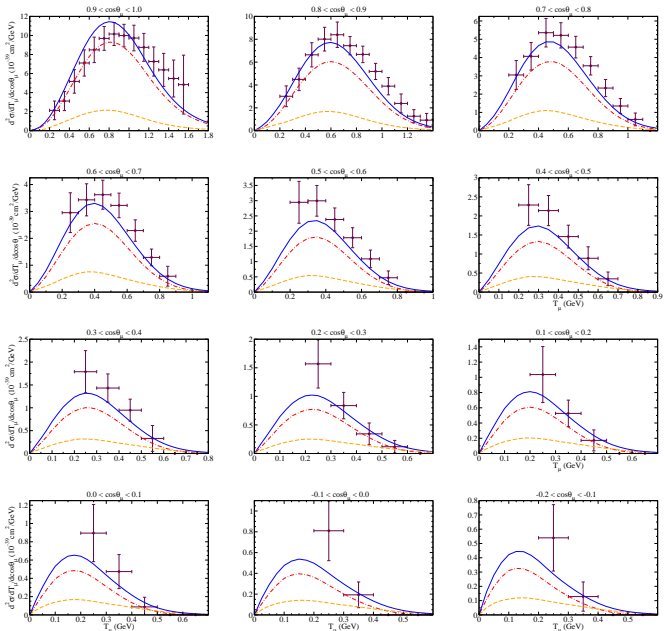
## Results

MiniBooNE  
CCQE-like  
DDCS  
 $\nu_\mu - C$

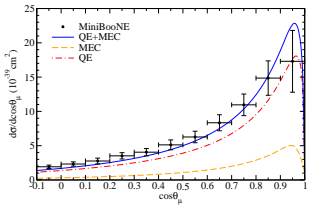
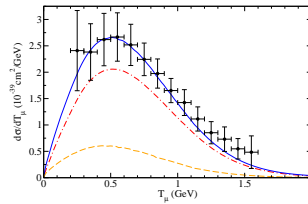
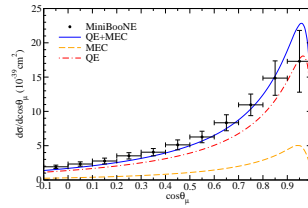
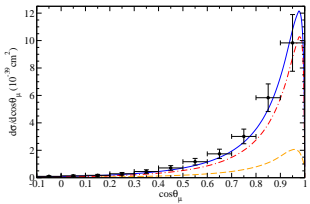


## Results

MiniBooNE  
CCQE-like  
DDCS  
 $\bar{\nu}_\mu - C$



# MiniBooNE CCQE-like single-differential cross sections

 $\nu_\mu - C$  $\bar{\nu}_\mu - C$ 

## Conclusions

- Validation against electron scattering data is the best possible test of nuclear models used in neutrino experiment analyses
- Superscaling is a valuable tool to connect electron and neutrino scattering
- MEC 2p2h excitations give sizeable contributions to  $\nu$ -A cross sections in the GeV region
- MEC 2p2h contributions violate scaling of both kinds: numerical studies show that the ratio 2body/1body roughly scales as  $k_F^3$
- Comparison of the SuSAv2+MEC model with inclusive electron scattering data on  $^{12}C$  and  $^{16}O$  is very satisfactory in a wide range of kinematics
- Fair agreement of the SuSAv2+MEC predictions with CCQE-like neutrino scattering data on  $^{12}C$  and  $^{16}O$
- Inclusive data are reproduced equally well by very different models: testing models in more exclusive channels is necessary
- Work in progress: extension to asymmetric nuclei, inclusive neutrino scattering including all inelasticities, semi-inclusive reactions

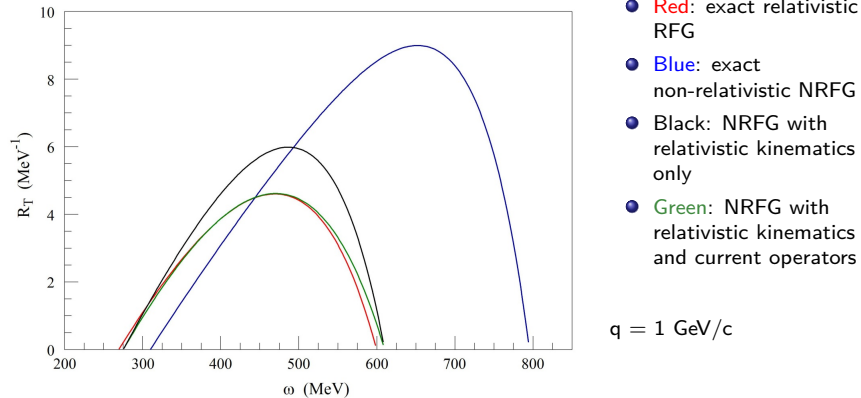
# Collaboration

J. Amaro (Granada)  
A. Antonov (Sofia)  
J. Caballero (Sevilla)  
A. De Pace (Torino)  
B. Donnelly (MIT)  
R. González-Jiménez (Ghent)  
M. Ivanov (Sofia)  
G. Megias (Sevilla)  
I. Ruiz Simo (Granada)  
J.M. Udías (Madrid)  
W. Van Orden (ODU)

Thank you

**Backup slides**

## Relativistic effects: kinematics and boosts



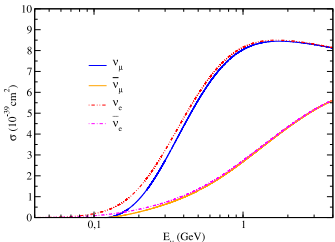


**Fig. 6.** (Color online.) SuSA predictions for muon (solid curves) and electron (dotted curves) neutrino and antineutrino CCQE cross section per nucleon on  $^{12}\text{C}$ .

to the two  $\tilde{M}_A$ -values used with the monopole axial-vector form factor is much larger than the one corresponding to the dipole parametrization. This is in accordance with previous results shown within the framework of parity-violating electron scattering [36]. We should notice that a dipole axial-vector form factor with  $M_A = 1.35 \text{ GeV}/c^2$  (in the SuSA model) produces a cross section that is slightly lower in the MiniBooNE energy region than that obtained using  $\tilde{M}_A = 1 \text{ GeV}/c^2$ , but gives a “reasonable (or a better)” explanation of the NOMAD data. On the other hand,  $\tilde{M}_A = 1 \text{ GeV}/c^2$  is probably not a good choice because the neutrino cross section keeps rising even at high energies. Indeed if one were to accept the monopole parametrization and fit the NOMAD data one would find that  $\tilde{M}_A = 0.70 \pm 0.06$  ( $0.72 \pm 0.14$ )  $\text{GeV}/c^2$  for neutrinos (antineutrinos). Old experiments with deuterium bubble chambers also performed fits of the data using a monopole axial form factor, obtaining  $\tilde{M}_A = 0.57 \pm 0.05$  [38] and  $\tilde{M}_A = 0.54 \pm 0.05$  [39]. While these studies would suggest that a dipole axial-vector form factor with the standard value of the dipole mass is preferred, given the modern interest in a potentially different behaviour, especially at high momentum transfers, new studies of neutrino disintegration of deuterium would be very valuable in clarifying this issue.

In Fig. 6 we compare the  $v_e$  ( $\bar{v}_e$ ) and  $v_\mu$  ( $\bar{v}_\mu$ ) cross sections in the SuSA model for the kinematics relevant for the proposed facility  $\nu$ STORM [29], which will provide high quality electron neutrino

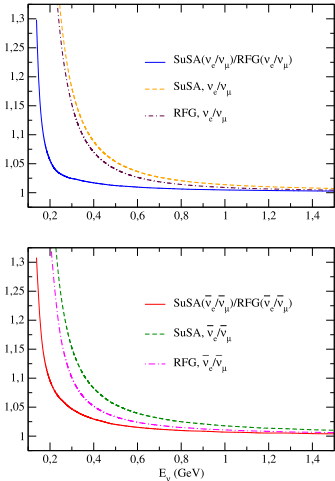


**Fig. 7.** (Color online.) Electron/muon neutrino (upper panel) and antineutrino (lower panel) CCQE cross section on  $^{12}\text{C}$  evaluated in the SuSA and RGF models.

allow one to extract new information concerning the electroweak nuclear matrix elements. It should be noted that the differences between RFG and SuSA in  $v_e/v_\mu$  ( $\bar{v}_e/\bar{v}_\mu$ ) (Fig. 7) are caused, at least partially, by the different theoretical descriptions of the nuclear responses employed in these models, specifically that the RFG scaling function is bounded and does not extend to large and small values of the scaling variable.

$$+ F_{\pi NN}(\mathbf{k}_1^2) F_{\pi N\Delta}(\mathbf{k}_1^2) F_{\pi NN}(\mathbf{k}_2^2) F_{\pi N\Delta}(\mathbf{k}_2^2) A^2 \frac{\mathbf{k}_1^2 T \mathbf{q}^2}{(\mathbf{k}_1^2 + \mu_\pi^2)(\mathbf{k}_2^2 + \mu_\pi^2)} \Big] \\ + (\leftrightarrow 1 \leftrightarrow 2) \Big\}, \quad (18)$$

where the first two terms on the right-hand side correspond to the diagrams (a)–(c) of Fig. 4, and the last one to the diagrams (d)–(f). In this case six distinct diagrams contribute.

In Eqs. (16), (17) and (18)  $k_L$  and  $k_T$  indicate the longitudinal and transverse components of the vector  $\mathbf{k}$  with respect to the direction fixed by  $\mathbf{q}$ . Furthermore, in the appropriate places, the hadronic monopole form factors

$$F_{\pi NN}(\mathbf{k}^2) = \frac{A_\pi^2 - \mu_\pi^2}{A_\pi^2 - \mathbf{k}^2}, \quad (19a)$$

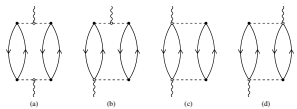


Fig. 2. The direct pionic contributions to the MEC 2p-2h response function.

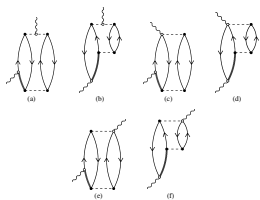


Fig. 3. The direct pionic/Δ interference contributions to the MEC 2p-2h response function.

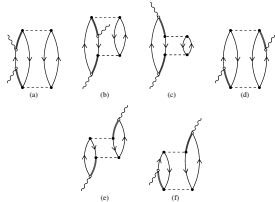


Fig. 4. The direct  $\Delta$  contributions to the MEC 2p-2h response function.

$$F_{\pi N\Delta}(\mathbf{k}^2) = \frac{A_{\pi N\Delta}^2}{A_{\pi N\Delta}^2 - \mathbf{k}^2} \quad (19b)$$

and the EM ones

$$F_{\gamma NN}(\mathbf{q}^2) = \frac{1}{(1 - \mathbf{q}^2/A_D^2)^2}, \quad (19c)$$

$$F_{\gamma N\Delta}(\mathbf{q}^2) = F_{\gamma NN}(\mathbf{q}^2) \left(1 - \frac{\mathbf{q}^2}{A_2^2}\right)^{-1/2} \left(1 - \frac{\mathbf{q}^2}{A_3^2}\right)^{-1/2} \quad (19d)$$

have been introduced. In the non-relativistic expressions the hadronic form factors have been taken in the static limit. The cut-offs have been chosen as in DBT, namely  $A_\pi = 1300$  MeV,  $A_{\pi N\Delta} = 1150$  MeV,  $A_D^2 = 0.71$  GeV $^2$ ,  $A_2 = M + M_A$  and  $A_3^2 = 3.5$  GeV $^2$ . This choice clearly makes it possible a direct comparison between our results for  $R_T$  and those of DBT.

For completeness, we give also the formulae of the (smaller) exchange contributions to the integrand of Eq. (15),  $\mathcal{R}_T^{E[\pi,\Delta]}(\mathbf{k}_1, \mathbf{k}_2; \mathbf{k}'_1, \mathbf{k}'_2; \mathbf{q}, \omega)$ , in the non-relativistic limit. The purely pionic contribution is identically zero, as a consequence of charge conservation and of the fact that the photon does not couple to a neutral pion. For the interference between pion and  $\Delta$  (Fig. 5) we have

$$\begin{aligned} & \mathcal{R}_T^{E[\pi,\Delta]}(\mathbf{k}_1, \mathbf{k}_2; \mathbf{k}'_1, \mathbf{k}'_2; \mathbf{q}, \omega) \\ &= \frac{V^4}{(2M)^4} \sum_{\sigma\tau} \sum_{ij} \left( \delta_{ij} - \frac{q_i q_j}{\mathbf{q}^2} \right) \left[ J_i^{\pi\sigma}(\mathbf{k}_1, \mathbf{k}_2) J_j^{\Delta}(\mathbf{k}'_1, \mathbf{k}'_2) \right. \\ & \quad \left. + J_i^{\Delta\sigma}(\mathbf{k}_1, \mathbf{k}_2) J_j^{\pi}(\mathbf{k}'_1, \mathbf{k}'_2) \right] \end{aligned}$$

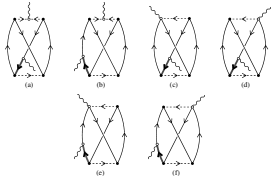


Fig. 5. The exchange pionic/Δ interference contributions to the MEC 2p-2h response function.

$$\begin{aligned}
 &= \frac{16 f_{\pi NN}^3 f_{\gamma\pi\pi}^2 f_{\gamma N\Delta} f_{\pi N\Delta}}{3\mu_\pi^4 M} \\
 &\times B q^2 \left[ \frac{(k_2 \times k'_2)^2}{(k_2^2 + \mu_\pi^2)(k'^2_2 + \mu_\pi^2)} \left[ \frac{1}{(k_1^2 + \mu_\pi^2)} + \frac{1}{k'^2_1 + \mu_\pi^2} \right] + (1 \leftrightarrow 2) \right] \\
 &+ \frac{8 f_{\pi NN}^2 f_{\pi N\Delta} f_{\gamma N\Delta} f_{\gamma N\Delta}}{3\mu_\Delta^4 M} \\
 &\times B \left\{ \frac{(q \cdot k_2)k_2^2 + (q \cdot k'_2)k_2^2 - (q \cdot k'_2)(k_2 \cdot k'_2) - (q \cdot k_2)(k_2 \cdot k'_2)}{(k_2^2 + \mu_\pi^2)(k'^2_2 + \mu_\pi^2)} \right. \\
 &+ \frac{(q \cdot k_1)k_1^2 - (q \cdot k'_1)(k_1 \cdot k'_1) + (q \cdot k'_1)k_1^2 - (q \cdot k_1)(k'_1 \cdot k_1)}{(k_1^2 + \mu_\pi^2)(k'^2_1 + \mu_\pi^2)} \\
 &\left. + (1 \leftrightarrow 2) \right\} \quad (20)
 \end{aligned}$$

The contribution of the  $\Delta$  alone (Fig. 6) is instead

$$\begin{aligned}
 &\mathcal{R}_T^{\Delta A}(k_1, k_2, k'_1, k'_2, q, \omega) \\
 &= \frac{V^4}{(2M)^4} \sum_{\sigma\tau} \sum_{ij} \left( \delta_{ij} - \frac{q_i q_j}{q^2} \right) J_i^{\sigma\tau}(k_1, k_2) J_j^{\sigma\tau}(k'_1, k'_2) \\
 &= \frac{4 f_{\pi NN}^2 f_{\pi N\Delta}^2 f_{\gamma N\Delta}^2}{9M^2 \mu_\Delta^4} q^2 \left[ B^2 \left[ \frac{(k_1 \cdot k'_1)(k_{1T} \cdot k'_{1T})}{(k_1^2 + \mu_\pi^2)(k'^2_1 + \mu_\pi^2)} + \frac{(k_1 \cdot k'_1)(k_{1T} \cdot k'_{1T})}{(k_1^2 + \mu_\pi^2)(k'^2_1 + \mu_\pi^2)} \right. \right. \\
 &\left. \left. + (1 \leftrightarrow 2) \right] + AB \left[ \frac{2(k_1 \times k'_1)^2 - 2k_{1L}k'_{1L}(k_1 \cdot k'_1) + k_{1L}^2 k_1^2 + k'_{1L}^2 k'_1^2}{(k_1^2 + \mu_\pi^2)(k'^2_1 + \mu_\pi^2)} \right. \right. \\
 &\left. \left. \times \frac{2(k_1 \times k'_2)^2 - 2k_{1L}k'_{2L}(k_1 \cdot k'_2) + k_{2L}^2 k_1^2 + k'_{2L}^2 k'_1^2}{(k_1^2 + \mu_\pi^2)(k'^2_2 + \mu_\pi^2)} \right. \right. \\
 &\left. \left. + (1 \leftrightarrow 2) \right] \right] \quad (21)
 \end{aligned}$$

Eqs. (16), (17) and (18) could in principle be compared with Eq. (5.11) of DBT; however, the overall normalization of the latter is not correct, since its dimension is not consistent with its definition (namely of being the transverse part of the amplitude  $\mathcal{T}$  given in Eq. (4.8) of DBT); moreover, the relative weights of the interference and  $\Delta$  contributions with respect to the pionic one differ, in our calculations, by a factor 2 and 4, respectively, from those of Eq. (5.11) of DBT. These factors, however, are not able to explain the marked difference between our results and those in that paper. Note that although the authors of DBT write down exactly the same expressions as we do for the non-relativistic MEC currents, actually they state that the non-relativistic procedure to get their Eq. (5.11) is applied at the level of the hadronic tensor, that is by reducing the (cumbersome) exact relativistic response.

In Fig. 7 we now compare our results with those of DBT, where the non-relativistic  $R_T$  (without the exchange contribution) is shown for  $q = 550$  MeV/c (left) and for  $q = 1140$  MeV/c (right), with an atomic mass number of 56 and utilizing a Fermi momentum  $k_F = 1.3$  fm $^{-1}$ . The latter value is employed for the sake of comparison with DBT, although in fact it is more appropriate for heavier nuclei.

It is clearly apparent in the figure that our predictions differ significantly from those of DBT: while the discrepancy is mild for moderate values of  $q$  (roughly, those encompassing the QEP), it becomes striking at higher energies, namely in the region of the so-called dip and of the  $\Delta$ -peak. Here our transverse response function in the proximity of the lightcone turns out to be larger by about a factor two at  $q = 550$  MeV/c and by over a factor three at  $q = 1140$  MeV/c.

Note that, in order to conform as closely as possible with the DBT approach, we have accounted for the initial state binding of the two holes by phenomenologically inserting

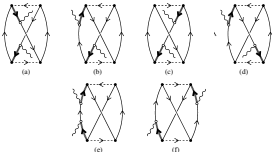


Fig. 6. The exchange  $\Delta$  contributions to the MEC 2p-2h response function.

## Numerical evaluation of the 2p2h hadronic tensor

$$W_{2p-2h}^{\mu\nu} = \frac{V}{(2\pi)^9} \int d^3 p'_1 d^3 h_1 d^3 h_2 \frac{M^4}{E_1 E_2 E'_1 E'_2} r^{\mu\nu}(p'_1, p'_2, h_1, h_2) \delta(E'_1 + E'_2 - E_1 - E_2 - \omega) \\ \times \theta(p'_2 - k_F) \theta(p'_1 - k_F) \theta(k_F - h_1) \theta(k_F - h_2)$$

where  $p'_2 = h_1 + h_2 + q - p'_1$  and the elementary hadronic tensor

$$r^{\mu\nu}(p'_1, p'_2, h_1, h_2) = \frac{1}{4} \sum_{s_1 s_2 s'_1 s'_2} \sum_{t_1 t_2 t'_1 t'_2} j^\mu(1', 2', 1, 2)_A^* j^\nu(1', 2', 1, 2)_A.$$

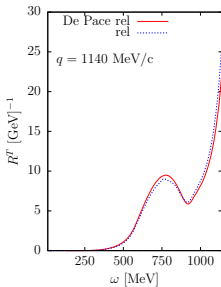
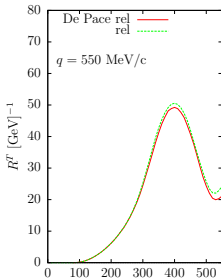
is given in terms of the antisymmetrized matrix element  $j^\mu(1', 2', 1, 2)_A$  of the 2-body current

$$j_{\text{MEC}}^\mu = j_{\text{sea}}^\mu + j_\pi^\mu + j_{\text{pole}}^\mu + j_\Delta^\mu$$

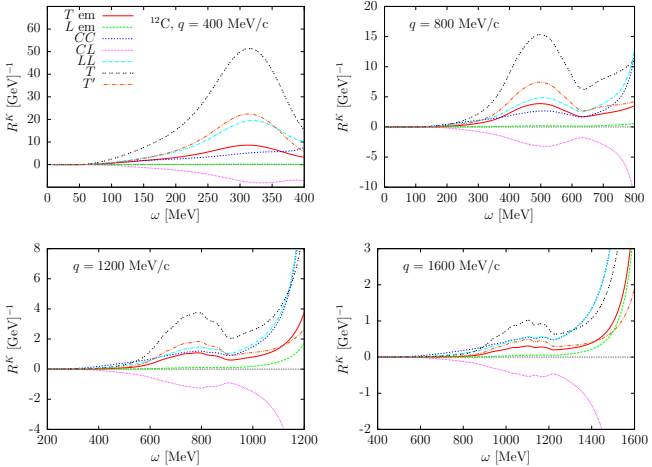
involving Dirac spinors,  $\gamma$  matrices, pion and  $\Delta$  propagators.

# Comparison between Amaro and De Pace calculations

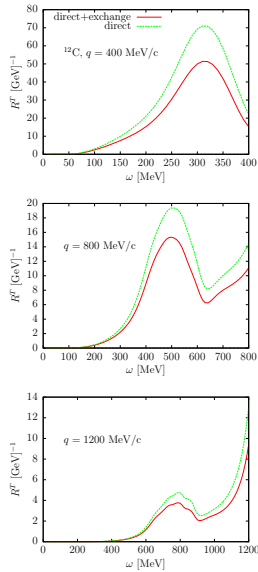
$^{56}\text{Fe}$



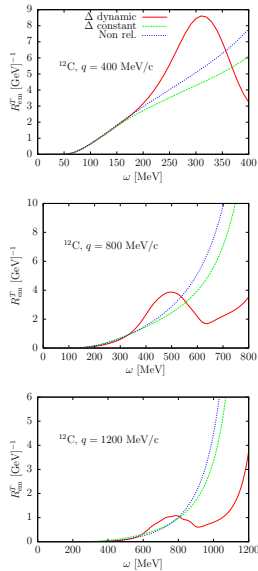
## Separated 2p2h responses



## Direct and exchange 2p2h responses

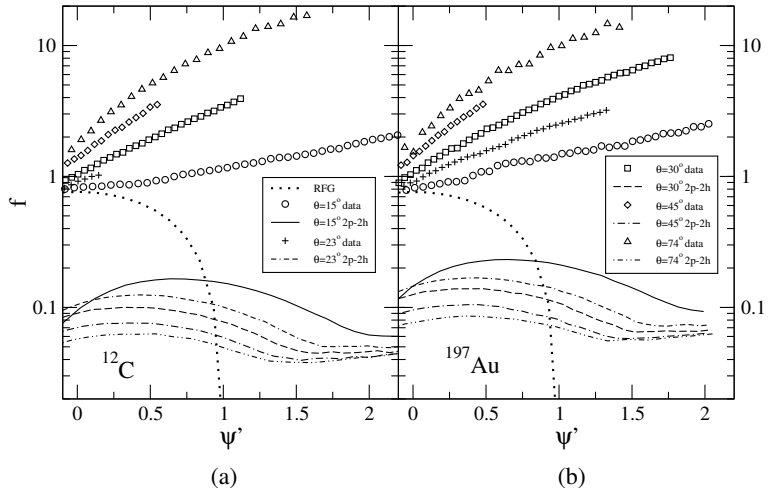


# Different treatments of the $\Delta$ propagator in the 2p2h response



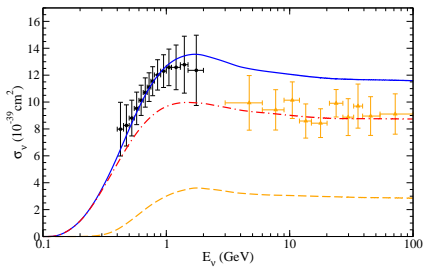
# The 2p2h MEC response for different nuclei and kinematics

- The 2p2h MEC response breaks scaling of both kinds

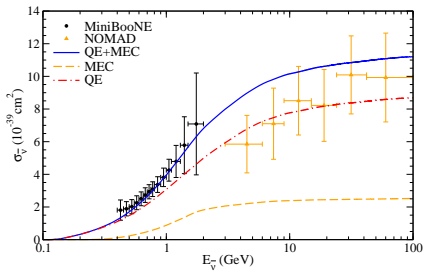


# MiniBooNE and NOMAD CCQE

$\nu_\mu - C$



$\bar{\nu}_\mu - C$



# The Relativistic Mean Field Model

- Ingredients:

- bound nucleon states are four-spinors, obtained from the self-consistent solution of the Dirac-Hartree equation, with underlying Walecka Lagrangian ( $\sigma$ ,  $\omega$  and  $\rho$  mesons);
- Final State Interactions (FSI) are included consistently: the outgoing nucleon is described by a relativistic w.f. obtained with the same scalar and vector potential used for the initial state.

- Results:

- good agreement with the phenomenological longitudinal scaling function;
- the transverse scaling function exhibits an enhancement of  $\sim 20\%$  with respect to the longitudinal one, in agreement with the analysis of separated L/T data;
- difference between the isoscalar and isovector components, of interest for CC neutrino reactions.

# $\psi$ -scaling variables

- QE:

$$\psi'_{\text{QE}}(q, \omega; k_F) \equiv \frac{1}{\sqrt{\xi_F}} \frac{\lambda' - \tau'}{\sqrt{(1 + \lambda')\tau' + \kappa\sqrt{\tau'(1 + \tau')}}},$$

$$\lambda' \equiv \frac{\omega'}{2m_N}, \quad \kappa \equiv \frac{q}{2m_N}, \quad \tau' \equiv \kappa^2 - \lambda'^2, \quad \omega' \equiv \omega - E^{\text{shift}}, \quad \xi_F \equiv \frac{E_F}{m_N} - 1$$

$E^{\text{shift}}$  is a parameter such that the maxima of QEP at different  $q$  align at  $\psi' = 0$ .

- 2p2h-MEC:

$$\psi'_{\text{MEC}}(q, \omega, k_F) \equiv \frac{1}{\sqrt{\xi_F^{\text{eff}}}} \frac{\lambda'_{\text{MEC}} - \tau'_{\text{MEC}} \rho'_{\text{MEC}}}{\sqrt{(1 + \lambda'_{\text{MEC}} \rho'_{\text{MEC}})\tau'_{\text{MEC}} + \kappa\sqrt{\tau'_{\text{MEC}}(1 + \tau'_{\text{MEC}} \rho'_{\text{MEC}}^2)}}},$$

$$\lambda'_{\text{MEC}} \equiv \frac{\omega'_{\text{MEC}}}{2m_N}, \quad \kappa \equiv \frac{q}{2m_N}, \quad \tau'_{\text{MEC}} \equiv \kappa^2 - (\lambda'_{\text{MEC}})^2,$$

$$\omega'_{\text{MEC}} \equiv \omega - E_{\text{MEC}}^{\text{shift}}, \quad \rho'_{\text{MEC}} \equiv 1 + \frac{1}{4\tau'_{\text{MEC}}} \left( \frac{m_*^2}{m_N^2} - 1 \right)$$

The parameters  $m_*$ ,  $\xi_F^{\text{eff}}$  and  $E_{\text{MEC}}^{\text{shift}}$  are chosen in such a way that the maxima of the 2p2h response at different values of  $q$  align at  $\psi'_{\text{MEC}} = 0$ .